Effect of Capillary Pressure on Phase Behavior in Tight Rocks and Shales

B. Nojabaei and **R.T. Johns,** SPE, Pennsylvania State University; and **L. Chu,** SPE, Hess Corporation

Summary

Phase behavior is important in the calculation of hydrocarbons in place and in the flow of phases through the rocks. Pore sizes can be on the order of nanometers for shale and tight-rock formations. Such small pores can affect the phase behavior of in-situ oil and gas because of increased capillary pressure. Not accounting for increased capillary pressure in small pores can lead to inaccurate estimates of ultimate recovery, and of saturation pressures. In this paper, capillary pressure is coupled with phase equilibrium equations, and the resulting system of nonlinear fugacity equations is solved to present a comprehensive examination of the effect of small pores on saturation pressures and fluid densities. Binary mixtures of methane with heavier hydrocarbons and a real reservoir fluid from the Bakken shale are considered.

The results show that accounting for the impact of small pore throats on pressure/volume/temperature (PVT) properties explains the inconsistent gas/oil-ratio (GOR) behavior, high flowing bottomhole pressures, and low gas-flow rate observed in the tight Bakken formation. The small pores decrease bubble-point pressures and either decrease or increase dew-point pressures, depending on which part of the two-phase envelope is examined. Large capillary pressure also decreases the oil density in situ, which affects the oil formation volume factor and ultimate reserves calculations. A good history match for wells in the middle Bakken formation is obtained only after considering a suppressed bubble-point pressure. The results show that the change in saturation pressures, fluid densities, and viscosities is highly dependent on the values of interfacial tension (IFT) (capillary pressure) used in the calculations.

Introduction

Low-permeability rocks and shale reservoirs are significant contributors to total oil and gas production in the US. These reservoirs are unique in that they have very low permeability, which requires long horizontal wells with multistage hydraulic fractures to generate productive flow rates. According to Kuila and Prasad (2011), the matrix in shale reservoirs consists of micropores smaller than 2 nm in diameter to mesopores with diameters in the range of 2 to 50 nm. Pores in shale reservoirs are associated with clay minerals and organic matter. Small pores increase capillary pressure, which can change saturation pressures and fluid densities.

Sigmund et al. (1973) investigated the effect of porous media on phase behavior of hydrocarbon binary mixtures both experimentally and numerically. Dew-point and bubble-point pressures were found to be the same in the 30- to 40-US-mesh glass-bead packing and in the absence of any porous media. In their theoretical work, they modeled capillary pressure by use of constant IFT and reported no significant difference in bubble-point and dew-point pressures except at high surface curvature. They concluded that such high curvature was unlikely to exist in reservoirs containing connate water because even where clay-sized particles are present, the finest pores would be occupied by connate water. Brusllovsky (1992) studied the effect of capillary pressure on phase equilibrium of a multicomponent system by use of a thermodynamic model. That author determined dew-point and bubble-point pressures in the presence of small pores for different values of pore radius and reported that when pores became smaller surface curvature increased and the bubble-point pressure decreased, whereas the dew-point pressure increased. They also concluded that in porous media with varying pore sizes, the bubble-point is reached first in the larger pores, whereas the dew-point occurs first in smaller pores. Further, they concluded that the influence of porous media on phase behavior for larger reservoir pressures is smaller. Ping et al. (1996) developed a theoretical model for calculating the dew-point by considering the effect of capillary pressure and adsorption in porous media. They showed that capillary pressure and adsorption increased the dew-point pressure. The increase in dew-point pressure increased with decreasing permeability and porosity. Zhilin et al. (2007a) proposed a new method for calculating oil/gas phase equilibrium in deep gas/condensate reservoirs. They calculated fluid and reservoir properties near the wellbore and concluded that interfacial phenomena and reservoir deformation increased the dew-point so that condensate appeared much earlier compared with the case with no IFT (zero capillary pressure). In other research by the same authors (Zhilin et al. 2007b), they developed models to predict dew-point pressure, retrograde liquid saturation during constant-volume depletion in the presence of IFT, gaseous formation water, and reservoir deformation. They concluded that interfacial phenomena and reservoir deformation increased dew-point pressure. Firincioglu et al. (2012) recently made flash calculations by use of the Peng-Robinson equation of state (Peng and Robinson 1976) (EOS) and included both surface and capillary forces. Their results show that surface forces are small compared with capillary forces for pores larger than approximately 1 nm.

All research to date has examined the effect of capillary pressure on only a portion of the phase envelope. In this paper, we examine the effect of large capillary pressure from nanometer-scale pores on the entire pressure/temperature (PT) phase envelope for various hydrocarbon mixtures, including the Bakken oil. We also include the effect of varying IFT on the saturation pressure, which approaches zero as the overall composition approaches a critical point. Further, we give field evidence from the Bakken shale of bubble-point pressure lowering caused by increased capillary pressure.

Model and Methodology

Vapor/liquid equilibrium is calculated considering only the effect of capillary pressure. We neglect adsorption and assume that molecular interactions with the surface and changes in fluid properties, such as density near the rock surface, are small. This assumption is likely satisfactory for pore sizes larger than 5 or 10 nm for molecules such as methane and water, which are typically on the order of 0.2 or 0.3 nm. Oils with larger molecules, such as *n*-decane (molecules approximately 1 nm in length), however, may require larger pore sizes for good phase-behavior prediction by use of the approach in this paper. Although we show results down to 1 nm in our figures, a more thorough analysis by use of molecular simulation or grand potential may bring new insight for the tiniest of pores (Evans et al. 1986; Restagno et al. 2000; Giovambattista et al. 2006). Nevertheless, given the uncertainty in surface roughness, pore geometries, and sizes within tight rocks, a practical macroscopic approach—such as the one presented here—is needed for use in history matching by adjusting the level of capillary pressure within the tight reservoir.

This paper (SPE 159258) was accepted for presentation at the SPE Annual Technical Conference and Exhibition, San Antonio, Texas, USA, 8–10 October 2012, and revised for publication. Original manuscript received for review 8 July 2012. Revised manuscript received for review 7 March 2013. Paper peer approved 29 April 2013.

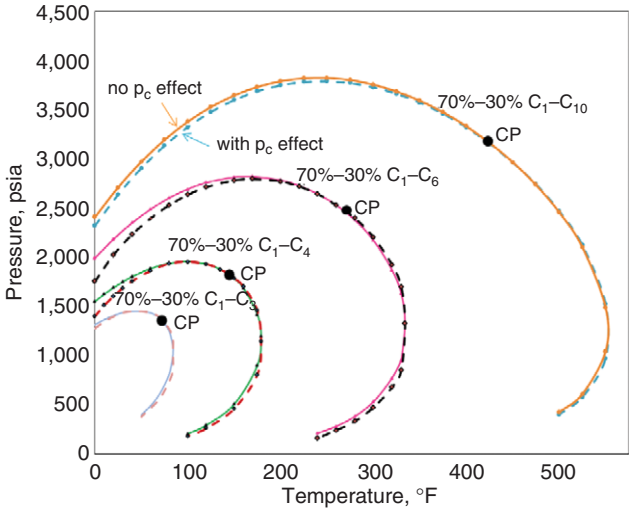

Fig. 1—Phase envelopes with and without capillary pressure for binary mixtures (70:30 C_1/C_4 and 70:30 C_1/C_6) and pore radius of 10 nm.

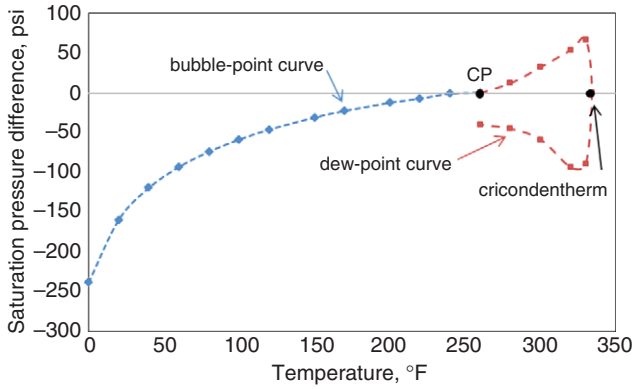

Fig. 2—Saturation-pressure differences for 70:30 C_1/C_6 mixture and pore radius of 10 nm.

Phase equilibrium is achieved by making the fugacity of each component across a liquid/vapor interface equal; the phase pressures at which the fugacities are evaluated therefore differ by the capillary pressure. Capillary pressure is calculated in this paper on the basis of the Young-Laplace equation in which the principle radii of curvature are equal, although it could alternatively be calculated on the basis of measured capillary pressure data for fluids of interest. Thus, we effectively evaluate the effect of capillary pressure on phase behavior only at the mean pore size of the porous medium. The following are satisfied at liquid/vapor equilibrium (Firoozabadi 1999):

$$P^V - P^L = p_c = \frac{2\sigma}{r} \quad \ldots\ldots\ldots\ldots\ldots\ldots\ldots\ldots\ldots\ldots (1)$$

$$f_i^V = f_i^L, \qquad i = 1 - N_c, \quad \ldots\ldots\ldots\ldots\ldots\ldots\ldots\ldots\ldots\ldots (2)$$

where r is taken to be the pore radius. Therefore, at the dew-point, we have

$$f_i^L(T, P^L, x_1 \ldots x_{N_c}) = f_i^V(T, P^V, z_1 \ldots z_{N_c}), \quad \ldots\ldots\ldots\ldots\ldots (3)$$

$$P^V - P^L = \frac{2\sigma}{r}, \quad \ldots\ldots\ldots\ldots\ldots\ldots\ldots\ldots\ldots\ldots (4)$$

and

$$\sum_{i=1}^{N_c} x_i = 1, \quad \ldots\ldots\ldots\ldots\ldots\ldots\ldots\ldots\ldots\ldots\ldots (5)$$

whereas at the bubble-point, we have

$$f_i^L(T, P^L, z_1 \ldots z_{N_c}) = f_i^V(T, P^V, y_1 \ldots y_{N_c}), \quad \ldots\ldots\ldots\ldots\ldots (6)$$

$$P^V - P^L = \frac{2\sigma}{r}, \quad \ldots\ldots\ldots\ldots\ldots\ldots\ldots\ldots\ldots\ldots (7)$$

and

$$\sum_{i=1}^{N_c} y_i = 1\,. \quad \ldots\ldots\ldots\ldots\ldots\ldots\ldots\ldots\ldots\ldots\ldots (8)$$

IFT changes as a function of composition by use of the Macleod and Sugden correlation (Pederson 2007). Therefore,

$$\sigma = \left[\sum_{i}^{N_c} \chi_i (x_i \overline{\rho}^L - y_i \overline{\rho}^V)\right]^4 \quad \ldots\ldots\ldots\ldots\ldots\ldots\ldots\ldots (9)$$

Thus, the IFT becomes zero at a critical point where the phase compositions and densities approach each other.

The system of equations for the bubble-point or dew-point calculation is solved by use of standard negative flash calculation procedures, in which successive substitution is initially used to update the K-values, followed by Newton iterations to convergence. The effect of capillary pressure on the saturation pressures is modeled by varying the pore radius from infinity (no capillary pressure) to a few nanometers. We use the Peng-Robinson EOS (Peng and Robinson 1976) in all calculations, although, as stated previously, we recognize that for very small pores (smaller than 10 nm) the approach used here may not adequately represent the molecular interactions within such a small pore and at the pore surface.

Results and Observations for Binary Mixtures

We first determine the PT phase envelopes for a variety of binary mixtures of C_1/C_n, where n is the number of carbon atoms. Binary interaction parameters are set to 0.005 for all the binary mixtures examined. Parachor coefficients are 77.33, 151.90, 191.70, 271.0, and 392.25 for C_1, C_3, C_4, C_6, and C_{10}, respectively. **Fig. 1** shows the phase envelopes with and without capillary pressure included for C_1/C_3, C_1/C_4, C_1/C_6, and C_1/C_{10} binary fluids at a fixed pore radius of 10 nm and a fixed mole fraction of 70% C_1. As is shown in Fig. 1 and **Fig. 2,** the capillary pressure reduces the bubble-point pressure over all temperatures, but the bubble-point suppression decreases to zero at the critical point. The figures also show that the effect of capillary pressure is more important at lower than at higher temperatures, although this is directly tied to the critical-point temperature. The effect on saturation pressures is relatively small in these examples because of the volatile fluids used. The change in bubble-point pressures generally increases as the fluids become more immiscible (C_3 is substituted with C_4, and C_4 with C_6) as long as the pressures remain relatively low. The effect of capillary pressure on bubble-point pressures, however, is decreased for the C_1/C_{10} mixture because the bubble-point pressures for that system become much larger, which reduces the density differences between liquid and vapor. The large pressures therefore reduce the IFT along the bubble-point curve by use of the correlation in Eq. 9.

Fig. 2 shows the dew-point and bubble-point saturation-pressure differences with and without capillary pressure for the C_1/C_6 fluid. The effect of capillary pressure on dew-point pressures is smaller than on bubble-point pressures. Capillary pressure increases dew-point pressures for the region where the dew-point pressures are greater than the cricondentherm, whereas it decreases the dew-point pressures for pressures lower than the cricondentherm. At the critical point, the dew-point is unchanged because, again, the IFT is zero there. Thus, there are two points on the phase envelope where the saturation pressures are unchanged, one at the critical point and the other at the cricondentherm. Our calculations further show that if parachor coefficients

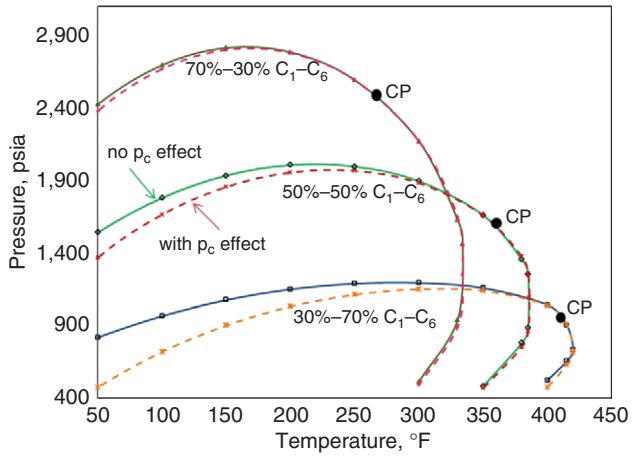

Fig. 3—Phase envelopes for various C_1/C_6 mixtures and pore radius of 20 nm.

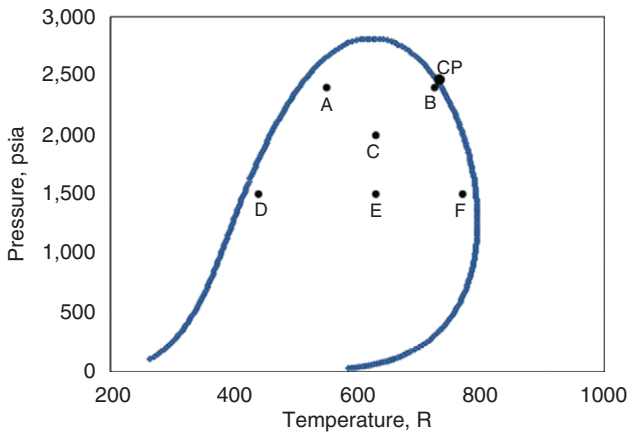

Fig. 4—Temperature and pressure points within the two-phase region for the 70:30 C_1/C_6 mixture used in the density calculations for Fig. 5.

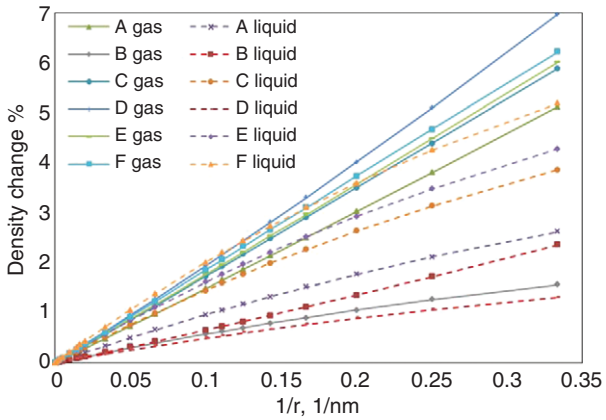

Fig. 5—Fluid densities for 70:30 C_1/C_6 mixture at PT points in Fig. 4.

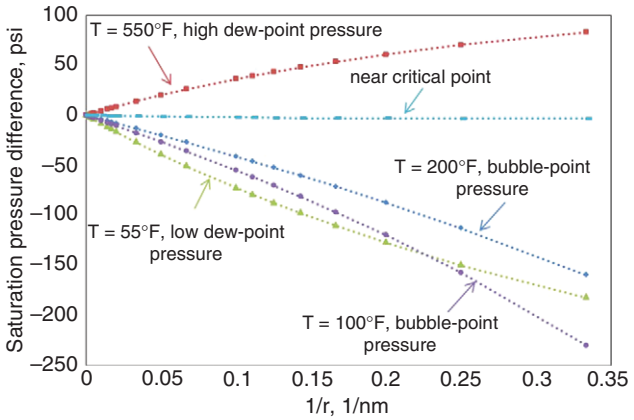

Fig. 6—Saturation-pressure differences [saturation pressure with capillary pressure (P_c) minus saturation pressure without P_c for a 70:30 C_1/C_{10} mixture].

are increased by only 10%, the decrease in bubble-point pressure at $T = 80°F$ for the C_1/C_6 fluid changes from 74 to 123 psi. This shows the significance of choosing proper parachor coefficients for flash calculations, and ultimately IFT, because they highly affect bubble-point pressures for nanopore reservoirs.

In **Fig. 3,** phase envelopes are plotted for different C_1/C_6 mixtures, whereas the pore radius is fixed at 20 nm. As shown, the heavier mixtures are more affected by capillary pressure at the same temperature. The more pronounced effect is because at a fixed temperature the heavier mixtures are generally further from the critical point and the bubble-point pressures are lower, increasing the vapor/liquid density difference and IFT through Eq. 9. As the fluids become heavier, the critical temperature and cricondentherm approach each other, decreasing the size of the region where dew-point pressures are increased by capillary pressure.

Fluid densities are also changed by capillary pressure, and in general, this effect for gas density increases as the pressure and temperature point moves within the two-phase region away from the dew-point-pressure curve and for liquid density as it moves away from the bubble-point-pressure curve. **Fig. 4** shows the two-phase envelope for the C_1/C_6 mixture. **Fig. 5** gives the change in densities for the phases that form at the PT points shown in Fig. 4 as a function of pore radius. As shown, both liquid and vapor density decrease as capillary pressure increases, but the magnitude of the change depends on the particular pressure and temperature point. Closer to the critical point, the decrease in fluid density becomes smaller, which is expected because capillary pressure there is zero. The maximum reduction observed for the selected points is 7% for vapor density and 5% for liquid density for the C_1/C_6 system. As capillary pressure increases, the percentage of C_1 increases in both liquid and vapor phases and, as a result, both vapor and liquid densities decrease.

The difference of saturation pressure with and without capillary pressure for the same C_1/C_{10} mixture as a function of pore size is shown in **Fig. 6.** Either an increase or decrease in the dew-point pressure is observed depending on the temperature (see Fig. 1 for two-phase envelope).

Fig. 7 gives the IFT by use of Eq. 9 as a function of pore radius for this same C_1/C_{10} mixture. The IFT increases as the pore

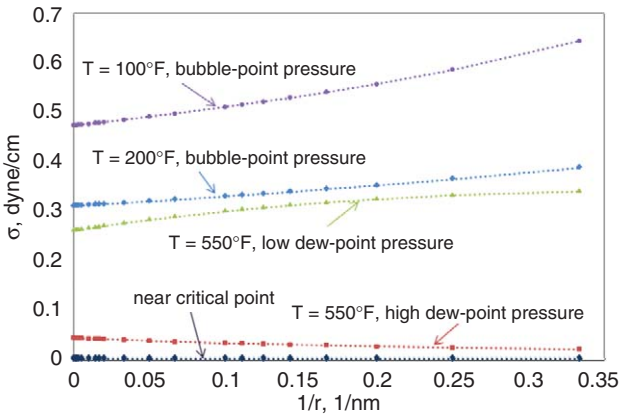

Fig. 7—IFT vs. pore curvature for a 70:30 C_1/C_{10} mixture.

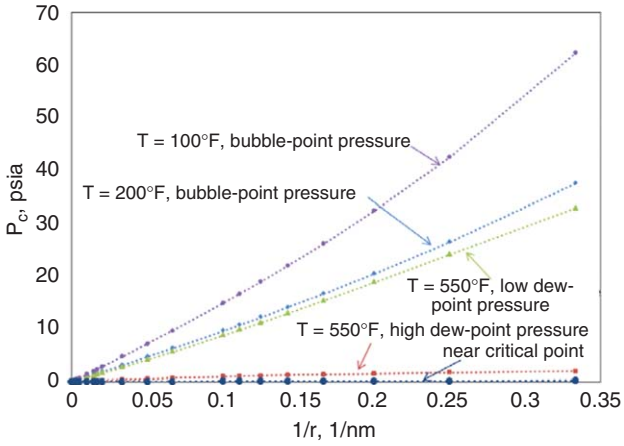

Fig. 8—Capillary pressures for a 70:30 C_1/C_{10} mixture.

size decreases because the fluid densities are changing. IFT increases farther from the critical point. The IFT is larger on the bubble-point curve than on the dew-point curve. Thus, the effect of capillary pressure on the bubble-point pressure is greater than it is for the dew-point pressure. The importance of IFT cannot be understated, and in this paper the IFTs from Eq. 9 were always small. We suggest that the IFTs should always be measured at several compositions with varying pressures and temperatures so that the expression for IFT can be properly tuned.

In **Fig. 8,** capillary pressure is plotted as a function of pore size for different temperatures for the C_1/C_{10} mixture by use of the IFTs shown in Fig. 7 and calculated with Eq. 1. The capillary pressure is not linear with pore size because the IFT depends on the pore size, which is coupled to fluid density. The capillary pressure is again zero at the critical point.

Results and Observations for Bakken Oil

In this section, we calculate the effect of capillary pressure on phase behavior for the Bakken shale oil. Bakken is an unconventional oil reservoir in the Williston basin. As shown in **Fig. 9,** the Williston basin is a large circular depression along the US/Canada border. It covers several hundred thousand square miles across parts of North Dakota, South Dakota, Montana, and the Canadian provinces of Manitoba and Saskatchewan. The Middle Bakken region, which is the main pay zone, consists of laminated tight limestone and siltstones sandwiched by two source rocks, the Upper and Lower Bakken shales. The porosity of the Middle Bakken region is approximately 6%, and the associated air permeability is on the order of microdarcies. Because of the relatively high initial water saturation and strong water wettability, the corresponding oil effective permeability is in the range of 30 to 100 nanodarcies. By use of the Kozeny-Carman equation (Kozeny 1927; Carman 1937), the corresponding pore-throat radius should be in the range of 10 to 40 nm. One of the typical pore-throat distributions estimated from high-pressure mercury/air capillary experiments is shown in **Fig. 10. Table 1** summarizes the key reservoir properties for Bakken. **Table 2** gives the input data required for the Peng-Robinson EOS calculations, and **Table 3** represents binary coefficients used for flash calculation of Bakken oil.

Fig. 11 shows the bubble-point-pressure curve for the Bakken fluid. As is shown, the effect of capillary pressure for the pore sizes of 10 and 20 nm decreases the bubble-point pressures more than in the binary mixtures, especially for the lower temperatures. In **Fig. 12,** bubble-point pressures are plotted vs. the pore curvature for different temperatures. For increasing temperatures, the bubble-point-pressure trend becomes flatter, indicating less effect of capillary pressure on the saturation curve. As temperature approaches the critical temperature, the slope becomes zero. At the reservoir temperature for the Bakken (240°F), the results show that there is only a 100-psi decrease in the bubble-point pressure for a pore size of 10 nm. This decrease is likely too low because the error in the estimated IFT by use of the Macleod and Sugden correlation generally increases as the pressure is reduced for a hydrocarbon fluid. Ayirala and Rao (2006) showed that measured IFTs were two to three times greater than those of the Macleod and Sugden correlation (Eq. 9) at moderate pressures. Further, the capillary pressure for gas/oil is a function of liquid saturation (Du and Chu 2012) and depends on wettability. Thus, the gas/oil capillary pressure in the Bakken is relatively uncertain. Fig. 12 shows that for an increase in the IFT by three times (multiplying Eq. 9 by three), the bubble-point pressure at reservoir temperature is reduced by approximately 150 psi for a pore radius of 20 nm and by 450 psi for a pore radius of 10 nm. This demonstrates the importance of possessing reliable IFT and capillary pressure measurements in liquid-rich shales. Although not considered here, adsorption could also suppress the bubble-point pressure further.

Fig. 13 gives the oil-density change as a function of pore size and pressure at a fixed temperature equal to the reservoir temperature (240°F) by use of the IFT values calculated with Eq. 9. The

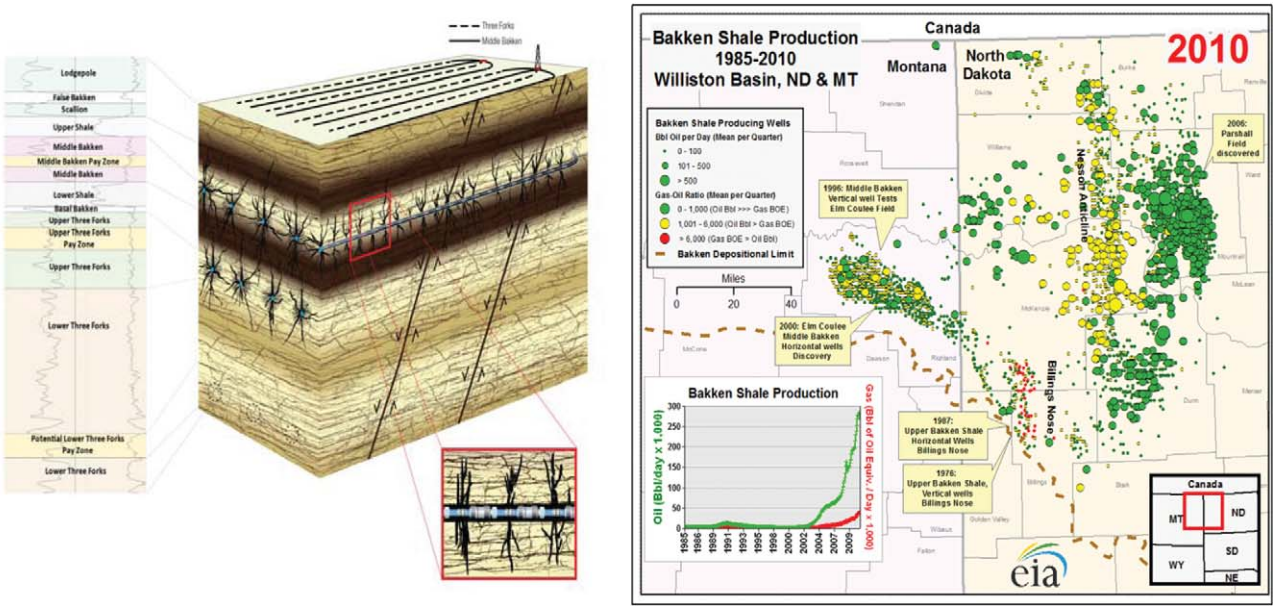

Fig. 9—Bakken reservoir in the Williston basin.

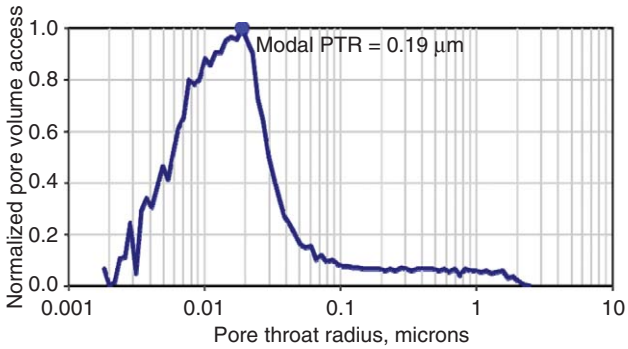

Fig. 10—Typical measured pore-throat-size distribution for middle Bakken from high-pressure mercury/air capillary pressure experiments.

results show that by decreasing the pore size, the oil density decreases significantly, thereby overestimating the oil density if the effect of capillary pressure is neglected. Similar to the saturation-pressure calculation, if the IFT were increased, the liquid density would be lowered significantly from these estimates. The liquid density at 1,500 psia and reservoir temperature decreases by approximately 1.0 to 3.4% for a pore size of 10 nm, and by 0.5 to 1.6% for a pore size of 20 nm. **Fig. 14** gives the change in oil viscosity as a function of pore size and pressure at reservoir temperature. The results show that the oil viscosity decreases for smaller pore sizes.

Pore Compressibility. The impact of pore radius on the PVT properties becomes more significant as the pore size decreases during pressure depletion. As is shown in **Fig. 15,** there is a significant reduction in the pore size of the Bakken shale because of an increase in effective stress as pore pressure decreases. The figure shows the upper and lower range in the pore-radius reduction, which were inferred from history matches on dozens of wells in the Bakken and analog laboratory data from the literature. By considering pore-size reduction caused by reservoir depletion, the reservoir is likely to experience even more reduction in bubble-point pressure throughout the life of the reservoir. **Fig. 16** shows the change in bubble-point pressure as a function of effective stress for four different initial pore sizes. For the pore radius of 10 nm, the calculations show that there is a reduction in the bubble-point pressure by more than 900 psi as the reservoir is depleted.

TABLE 1—RESERVOIR PROPERTIES FOR BAKKEN

Property	Measurement	Unit
Sample depth	9,500	ft (measured depth)
Reservoir pressure	6,840	psia
Reservoir temperature	240	°F
Modal range for pore size	10 to 50	nm

Production-Well Data. The results described previously have been used in the Bakken reservoir for adjusting the PVT properties and assessing the corresponding impact on the well performance and ultimate reserves.

Because of the impact of the nanopores on the fluid/rock properties, several anomalous fluid-flow phenomena have been observed in many Bakken wells, although the corresponding physics behind them has not been fully understood. One such aberration is the long-lasting flat GOR with or without the short stepwise jump observed in many Bakken wells, as shown in **Figs. 17a and 17b.**

Fig. 17a shows the producing GOR (R_p) for Well F, a typical multistage-fractured horizontal well in the Middle Bakken. The buildup data and pressure measurements from the observation wells revealed that both the flowing bottomhole pressure and the pressure around the wells have been below the bubble-point pressure, but the R_p values during the 4 years of production are still close to the initial GOR (R_{si}). Such GOR behavior could not be matched with the PVT properties reported by the laboratory. There are two realistic scenarios that may create the flattened GOR even when the reservoir pressure is well below the bubble-point pressure: enhanced critical gas saturation in tight rocks and

TABLE 2—COMPOSITIONAL DATA FOR BAKKEN OIL

Component	Molar Fraction	Critical Pressure (psia)	Critical Temperature (R)	Acentric Factor	Molar Weight (lbm/lbm mol)	Critical Volume (ft/lbm mol)	Parachor Coefficient
C_1	0.36736	655.02	335.336	0.0102	16.535	1.58	74.8
C_2	0.14885	721.99	549.969	0.1028	30.433	2.34	107.7
C_3	0.09334	615.76	665.97	0.152	44.097	3.25	151.9
C_4	0.05751	546.46	759.208	0.1894	58.124	4.11	189.6
C_5–C_6	0.06406	461.29	875.479	0.2684	78.295	5.39	250.2
C_7–C_{12}	0.15854	363.34	1053.25	0.4291	120.562	8.81	350.2
C_{13}–C_{21}	0.0733	249.61	1332.095	0.7203	220.716	15.19	590.0
C_{22}–C_{80}	0.03704	190.12	1844.491	1.0159	443.518	36	1216.8

TABLE 3—BINARY INTERACTION PARAMETERS FOR BAKKEN OIL

	C_1	C_2	C_3	C_4	C_5–C_6	C_7–C_{12}	C_{13}–C_{21}	C_{22}–C_{80}
C_1	0	0.005	0.0035	0.0035	0.0037	0.0033	0.0033	0.0033
C_2	0.005	0	0.0031	0.0031	0.0031	0.0026	0.0026	0.0026
C_3	0.0035	0.0031	0	0	0	0	0	0
C_4	0.0035	0.0031	0	0	0	0	0	0
C_5–C_6	0.0037	0.0031	0	0	0	0	0	0
C_7–C_{12}	0.0033	0.0026	0	0	0	0	0	0
C_{13}–C_{21}	0.0033	0.0026	0	0	0	0	0	0
C_{22}–C_{80}	0.0033	0.0026	0	0	0	0	0	0

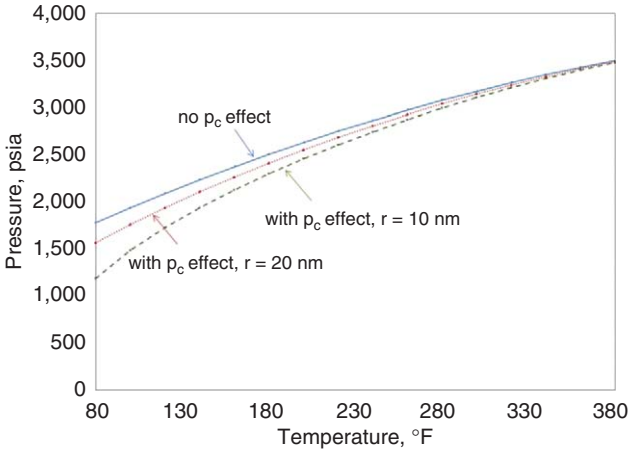

Fig. 11—Bubble-point pressures for Bakken oil.

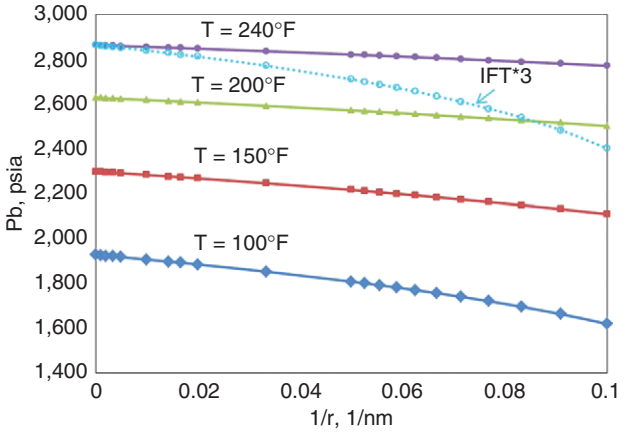

Fig. 12—Bubble-point pressure vs. pore curvature for Bakken fluid.

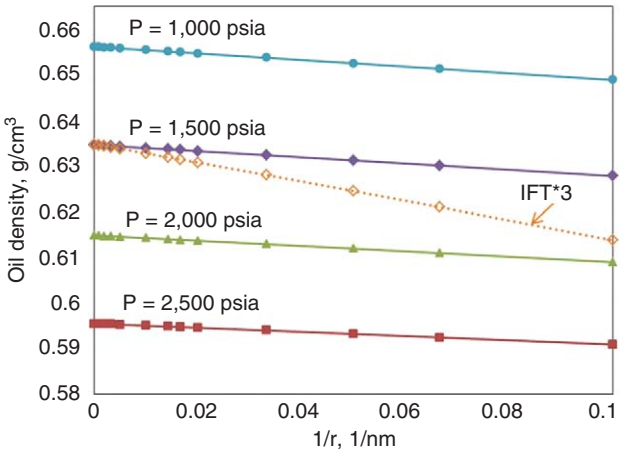

Fig. 13—Liquid density for the Bakken fluid at the reservoir temperature of 240°F.

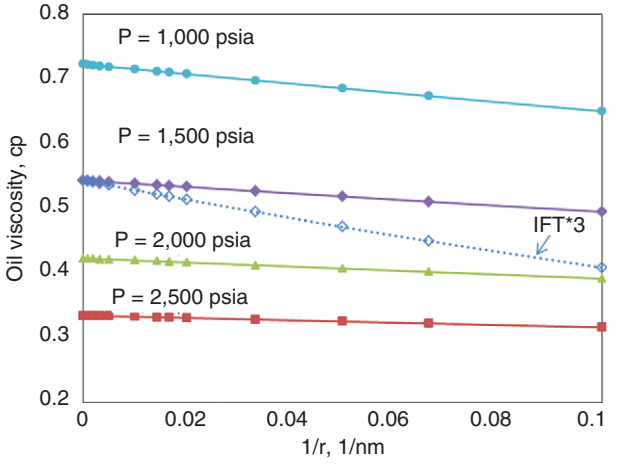

Fig. 14—Liquid viscosity for the Bakken fluid at the reservoir temperature of 240°F.

suppressed bubble-point pressure caused by the tiny pore sizes. The expected behaviors of GOR with time, however, for those two scenarios are different. Simulations show that large critical gas saturation alone cannot explain the gas production history observed in the Bakken. In general, a higher critical gas-saturation will decrease the GOR for some time, but will then be followed by a large jump in GOR (by several orders of magnitude) after reaching the critical saturation. If the bubble-point pressure is suppressed so that the reservoir pressure always exceeds the bubble-point pressure, then gas does not evolve at all in the reservoir. The combination of the higher critical gas saturation and suppressed bubble-point pressure will give a long period of a relatively flat GOR associated with some smaller fluctuations, as shown in Fig. 17. Depending on the location in the Bakken, the GOR ranges from 507 to 1,712 scf/bbl, whereas the bubble-point pressure varies from 1,617 to 3,403 psi. Our operational flowing bottomhole pressures are far below the bubble-point pressure for a substantial flow period, and we have not observed any increased

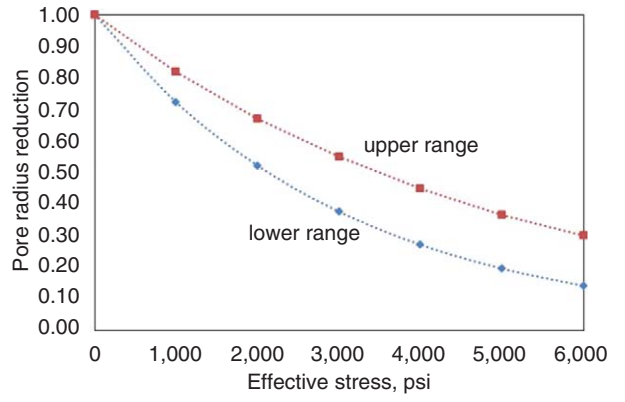

Fig. 15—Pore-radius reduction caused by the compaction effect.

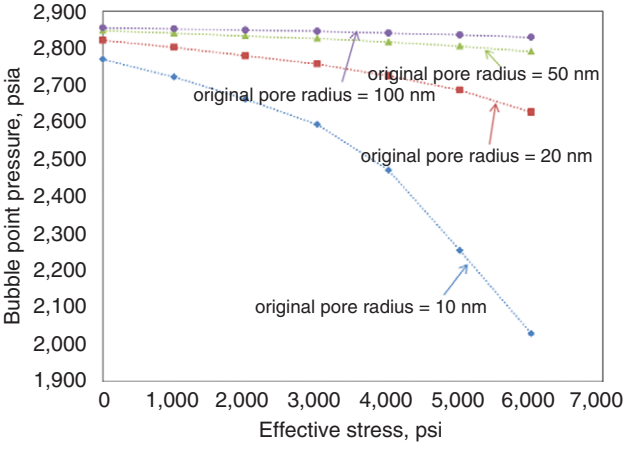

Fig. 16—Bubble-point-pressure reduction caused by the compaction effect.

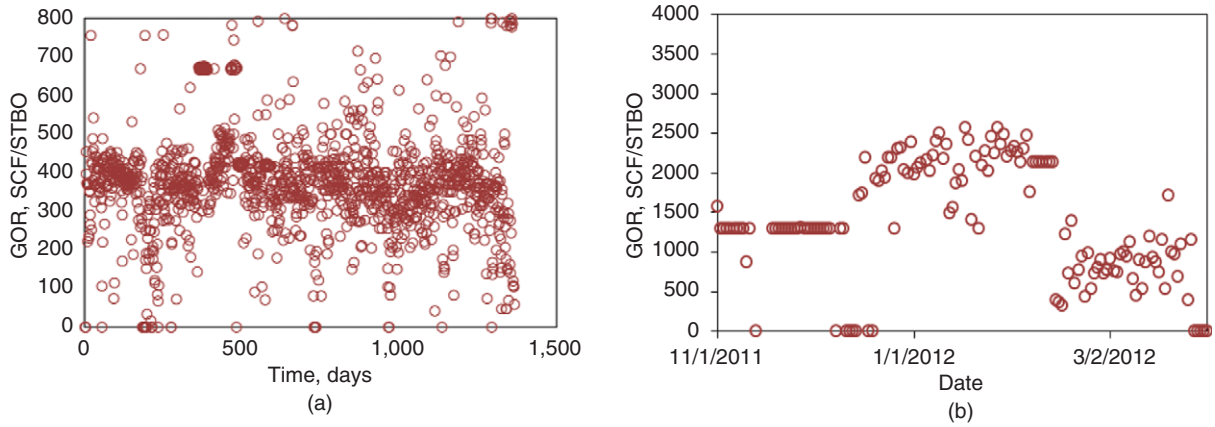

Fig. 17—(a) Producing GOR for Well F. (b) Producing GOR for Well A.

GOR. The only method to match this behavior is to include a suppressed bubble-point pressure in the simulations.

Real-world cases could be further complicated by pore compressibility, water-saturation changes, and the high critical gas saturation associated with tiny pore throats. As the depletion progresses, the bubble-point pressure and liquid-phase density will continue dropping because of the pore-size decrease caused by increased effective stress. Therefore, each reduction is not a constant drop, but rather a function of the depletion process. Water in water-wet reservoirs occupies the smaller pores and may cause increased oil/gas capillary pressure, which may result in even more suppression of the bubble-point pressure. Extremely high critical gas saturation could delay the formation of a continuous gas phase. According to Byrnes (2003), the critical gas saturation in nanodarcy-order-permeability rock could reach 30%.

On the basis of the previous discussions, we can describe the complexity of the phase behavior and saturation distribution in a nanopore reservoir. As the depletion process progresses, there may exist two-phase regions in parts of the reservoir and liquid-phase-only regions in other parts of the reservoir, depending on the associated pore sizes and depletion process. Even within the two-phase regions, the accumulated free gas will not flow until it reaches the corresponding critical gas saturation and forms a continuous phase. The gas phase may stop flowing again if the gas saturation drops below the critical level after a short period of time. The combination of the bubble-point-pressure suppression and high critical gas saturation may explain the short timestep-wise GOR increase observed in some of the Middle Bakken wells. Understanding and correctly capturing the heterogeneity and impact of tiny pores on the PVT properties and phase behavior could greatly facilitate the history match and allow a reliable well-performance forecast and reserves assessment.

Figs. 18 and 19 show the history match of the daily gas-flow rate and of flowing bottomhole pressure for Well R in the Middle Bakken region, respectively. Just after 4 months of production, free-gas production took place for the scenario with original PVT properties, as demonstrated by the green rectangles in Fig. 18. Accordingly, as shown in Fig. 19, the corresponding flowing bottomhole pressures for the scenario with original bubble-point pressure are much lower than the historical ones because of the increased gas production and higher oil viscosity. Both the flowing bottomhole pressure and the daily gas rate match the historical data well after adjusting the PVT properties (labeled as Suppressed Pb, with Pb being bubble-point pressure in both figures).

Such adjustment of the PVT properties makes a significant impact on both production profile and the ultimate reserves, as shown in **Fig. 20.** Although the production profiles in the early period are different for the scenarios of liquid phase only and suppressed bubble-point pressure, the corresponding ultimate reserves are similar. On the other hand, both the production profile and the ultimate reserves associated with the scenario of original PVT properties are substantially different from the previous

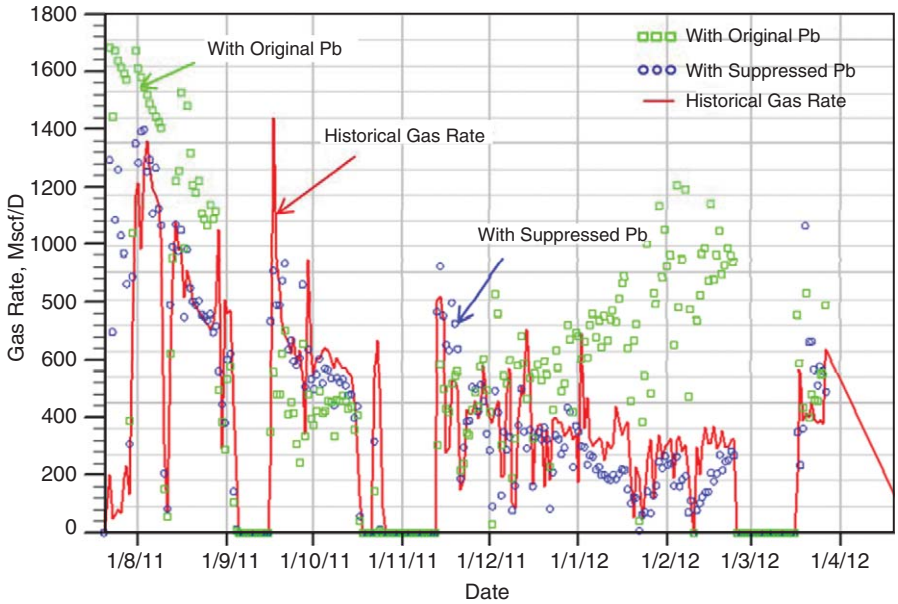

Fig. 18—History match of flowing bottomhole pressure for the scenarios with or without PVT adjustment.

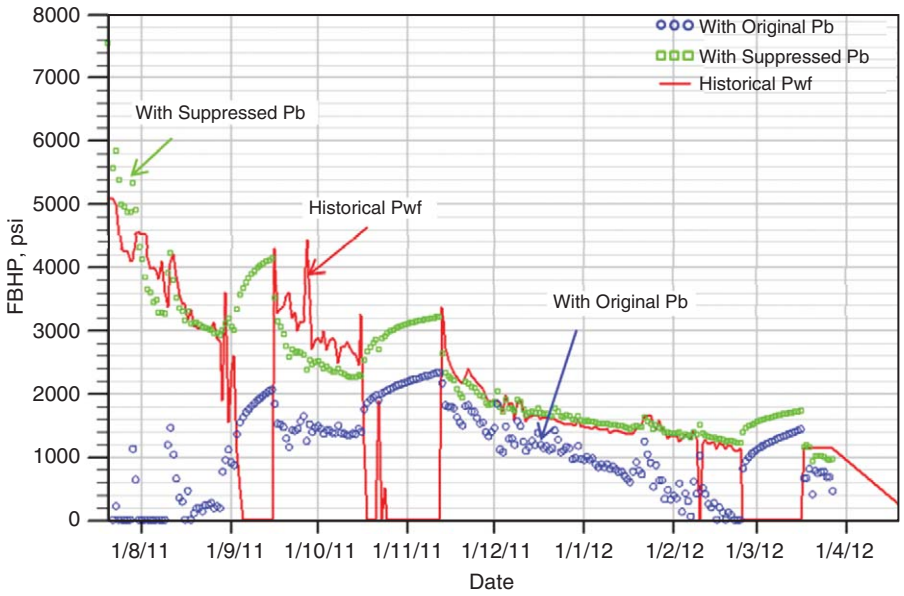

Fig. 19—History match of gas rate for the scenarios with or without PVT adjustment.

two cases. The reserves difference between the two cases is 30%. The scenario with the suppressed bubble-point pressure allows for widening the favored operation window and enhancing the well economics.

Summary and Conclusions

Tiny pores in many tight rocks and shale reservoirs can cause changes in phase behavior of hydrocarbons because of capillary pressure. As this research shows, this change caused by small pores is negligible unless the pore radius is on the order of tens of nanometers. For tight oil reservoirs, this effect should be considered to obtain better estimates of saturation pressure and fluid density, which leads to more-accurate estimates of ultimate reserves. Additional research should be performed in the future to include the effect of adsorption and fluid structure on equilibrium phase behavior within the tiniest of pores.

By considering the effect of capillary pressure caused by small pores, bubble-point pressure decreases and there is either a decrease or increase in dew-point pressure, depending on the location on the phase envelope. Capillary pressure mostly influences bubble-point pressure rather than the dew-point pressure. Dew-point pressures increase when the pressure is greater than the pressure evaluated at the cricondentherm, but decrease at pressures lower than the cricondentherm pressure. The change in saturation pressures increases for heavier mixtures and when the bubble-point pressure is smaller. There is no change in saturation pressure or fluid densities at the critical point, where IFT is zero. The results in this paper highlight the importance of measuring IFT and pore-size reductions with pressure, because both of these can greatly affect the impact of capillary pressure on saturation pressures, phase densities, and viscosities.

For the Bakken shale, the reduction of bubble-point pressure caused by small pores and high critical gas saturation in tight reservoirs can explain why there is no increase in producing GORs. History matching of flowing bottomhole pressure and flow rate is more accurate when the effect of capillary pressure is considered. This effect can strongly affect the estimation of ultimate recovery and future hydrocarbon production.

Nomenclature

f = fugacity
N_c = number of components
P = pressure, psia
r = pore radius, nm

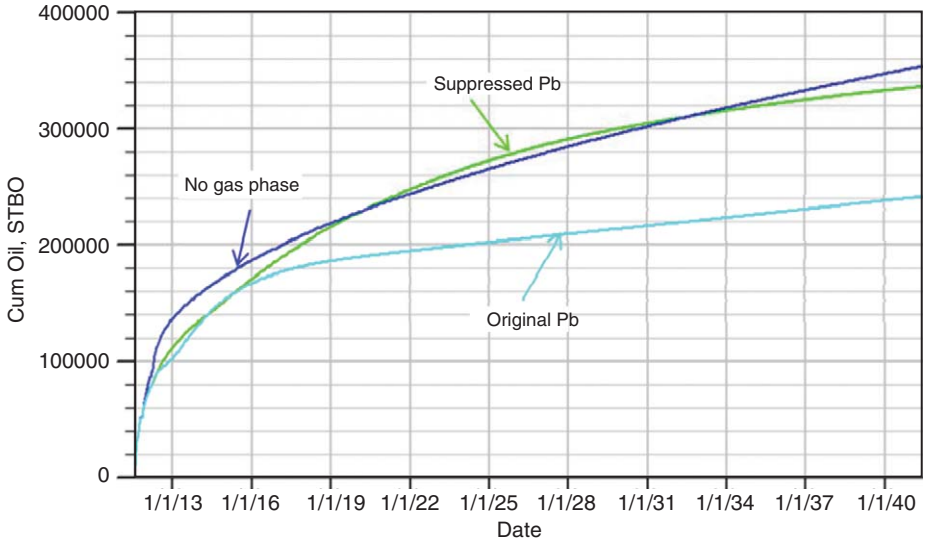

Fig. 20—Impact of the PVT properties on the ultimate reserves.

R_p = producing gas/oil ratio
R_{si} = initial gas/oil ratio
T = temperature, °F or R
x = molar fraction in liquid phase
y = molar fraction in vapor phase
z = molar fraction in total fluid system
μ = chemical potential, cp
ρ = density, g/cm^3 or lbm/ft^3
σ = interfacial tension, dyne/cm
χ = parachor
$\overline{\rho}$ = molar density, lbm/lbmol

Superscripts

L = liquid phase
V = vapor phase

Subscripts

i = component identification
n = number of carbon atoms

Acknowledgments

This research was partly sponsored by the Unconventional Natural Resources Consortium and the Gas Flooding Research Consortium at the EMS Energy Institute at Pennsylvania State University. We also thank the Hess Corporation for permission to publish this paper, and Gary Pope at the University of Texas at Austin for suggesting this topic.

References

Ayirala, S. C. and Rao, D. N. 2006. A New Parachor Model to Predict Dynamic Interfacial Tension and Miscibility in Multicomponent Hydrocarbon Systems. *J. Colloid Interf. Sci.* **299** (1): 321–331. http://dx.doi.org/10.1016/j.jcis.2006.12.030.

Brusllovsky, A. L. 1992. Mathematical Simulation of Phase Behavior of Natural Multicomponent Systems at High Pressure with an Equation of State. *SPE Res Eng* **7** (1): 117–122. http://dx.doi.org/10.2118/20180-PA.

Byrnes, A. P. 2003. Aspects of Permeability, Capillary Pressure, and Relative Permeability Properties and Distribution in Low-Permeability Rocks Important to Evaluation, Damage, and Stimulation. Proc., Rocky Mountain Association of Geologists Petroleum Systems and Reservoirs of Southwest Wyoming Symposium, Denver, Colorado, 19 September.

Carman, P. C. 1937. Fluid Flow Through Granular Beds. *T. I. Chem. Eng.-Lond.* **15:** 150–166.

Du, L. and Chu, L. 2012. Understanding Anomalous Phase Behavior in Unconventional Oil Reservoirs. Paper SPE 161830 presented at SPE Canadian Unconventional Resources Conference, Calgary, Alberta, Canada, 30 October–1 November. http://dx.doi.org/10.2118/161830-MS.

Evans, R., Marconi, U. M. B. and Tarazona, P. 1986. Fluids in Narrow Pores: Adsorption, Capillary Condensation, and Critical Points. *J. Chem. Phys.* **84** (4): 2376–2399. http://link.aip.org/link/doi/10.1063/1.450352.

Firincioglu, T., Ozkan E. and Ozgen, C. 2012. Thermodynamics of Multiphase Flow in Unconventional Liquids-Rich Reservoirs Paper SPE 159869 presented at the SPE Annual Technical Conference and Exhibition, San Antonio, Texas, 8–10 October. http://dx.doi.org/10.2118/159869-MS.

Firoozabadi, A. 1999. *Thermodynamics of Hydrocarbon Reservoirs.* New York City, New York: McGraw-Hill.

Giovambattista, N., Rossky, P. J. and Debenedetti, G. 2006. Effect of Pressure on the Phase Behavior and Structure of Water Confined Between Nanoscale Hydrophobic and Hydrophilic Plates. *Phys. Rev. E* **73** (4): 1,604–1,618. http://dx.doi.org/10.1103/PhysRevE.73.041604.

Kozeny, J. 1927. Über Kapillare Leitung des Wassers im Boden. *Sitzungsberichte der Akademie der Wissenschaften, Wien* **136** (2a): 271–306.

Kuila, U. and Prasad, M. 2011. Surface Area and Pore-Size Distribution in Clays and Shales. Paper SPE 146869 presented at the SPE Annual Technical Conference and Exhibition, Denver, Colorado, 30 October–2 November. http://dx.doi.org/10.2118/146869-MS.

Pedersen K.S., Christensen P.L., Phase Behavior of Petroleum Reservoir Fluids, CRC Press, Taylor & Francis Group, 2007.

Peng, D. Y., and Robinson, D. B. 1976. A New Two-Constant Equation of State. *Ind. Eng. Chem. Fundamen.* **15** (1): 59–64. http://dx.doi.org/10.1021/i160057a011.

Ping, G., Liangtian, S., Li, S., et al. 1996. A Theoretical Study of the Effect of Porous Media on the Dew Point Pressure of a Gas Condensate. Paper SPE 35644 presented at SPE Gas Technology Symposium, Calgary, Alberta, Canada, 28 April–1 May. http://dx.doi.org/10.2118/35644-MS.

Restagno, F., Bocquet, L. and Biben, T. 2000. Metastability and Nucleation in Capillary Condensation. *Phys. Rev. Lett.* **84** (11): 2433–2436. http://dx.doi.org/10.1103/PhysRevLett.84.2433.

Sigmund, P. M., Dranchuk, P. M., Morrow, N. R., et al. 1973. Retrograde Condensation in Porous Media. *SPE J.* **13** (2): 93–104. http://dx.doi.org/10.2118/3476-PA.

Zhilin, Q., Wang, S., Du, Z., et a. 2007a. A New Approach for Phase Behavior and Well Productivity Studies in the Deep Gas-Condensate Reservoir with Low Permeability. Paper SPE 106750 presented at Production and Operations Symposium, Oklahoma City, Oklahoma, 31 March–3 April. http://dx.doi.org/10.2118/106750-MS.

Zhilin, Q., Du, Z., Liang, B., et al. 2007b. Phase Behavior Study in the Deep Gas-Condensate Reservoir with Low Permeability. Paper SPE 107315 presented at the EUROPEC/EAGE Conference and Exhibition, London, UK, 11–14 June. http://dx.doi.org/10.2118/107315-MS.

Bahareh Nojabaei is a PhD candidate in petroleum and natural gas engineering at Pennsylvania State University, University Park, Pennsylvania. Her research areas include reservoir simulation and well testing in unconventional reservoirs, diagnostic fracture injection testing analysis, and phase behavior in tight rocks. Nojabaei earned an MS degree in mechanical engineering from Tehran Polytechnic University, Iran, and a BS degree from Iran University of Science and Technology.

Russell Taylor Johns is Professor of Petroleum and Natural Gas Engineering in the Department of Energy and Mineral Engineering at Pennsylvania State University, where he holds the Victor and Anna Mae Beghini Faculty Fellowship. Before his current position, he served on the faculty at the University of Texas at Austin from 1995 to 2010. Johns also has 9 years of industrial experience as a petrophysical engineer with Shell Oil and as a consulting engineer for Colenco Power Consulting in Baden, Switzerland. He holds a BS degree in electrical engineering from Northwestern University and MS and PhD degrees in petroleum engineering from Stanford University. Johns' research interests include enhanced oil recovery, unconventional gas engineering, theory of gas-injection processes, multiphase flow in porous media, and well testing. In these areas, he has published more than 160 technical papers, reports, and books. Johns received the 1993 SPE Ferguson Medal for his research on the combined condensing/vaporizing gasdrive process. He also received the SPE Faculty Excellence award in 1997, the Young Faculty award from the University of Texas in 2000, and the departmental teaching award in 2004. Johns served as co-Executive Editor for *SPE Reservoir Evaluation and Engineering* from 2002 to 2004. In 2009, he was awarded SPE Distinguished Member status. Johns is currently an associate editor for *SPE Journal* and director of the Gas Flooding Consortium and co-Director of the Unconventional Natural Resources Consortium at Pennsylvania State University.

Lifu Chu is a senior reservoir engineering adviser in EPT, Hess Corporation. He previously worked for Devon Energy, Total, and the University of Tulsa. Chu's working interests include integrated reservoir characterization, simulation, pressure-transient analysis and rate-transient analysis. In his recent work with Hess, he has focused on new technology developments for unconventional resources. Chu holds a BS degree in chemical and mechanical engineering from Daqing Petroleum Institute, Daqing, China; an MS degree in petroleum engineering from Texas Tech University; and a PhD degree in petroleum and natural gas engineering from Pennsylvania State University. He has served on the SPE Pressure Transient Technical Committee, Reservoir Characterization Steering Committee, and Technical Review Committee.